

# A Study on Intravascular Ultrasound Image Processing

Esmeraldo dos Santos Filho<sup>1</sup>, Makoto Yoshizawa<sup>2</sup>, Akira Tanaka<sup>3</sup> and Yoshifumi Saijo<sup>4</sup>

1 Graduate School of Engineering, Tohoku University

2 Information Synergy Center, Tohoku University

3 College of Symbiotic Systems Science, Fukushima University

4 Institute of Development, Aging and Cancer, Tohoku University

Esmeraldo dos Santos Filho: Tohoku University – Graduate School of Engineering, Sendai-shi, Aoba-ku, Aoba-yama 05, 980-8579. Email: [esmeraldo@ieee.org](mailto:esmeraldo@ieee.org)

**Abstract**—Innovative applications of image processing techniques for analysis of intravascular ultrasound images are presented. This work has two main objectives: (1) to detect the luminal contour which is necessary to assess the degree of vessel stenosis, and (2) to detect presence of calcification, which is an important information for definition of the intervention method. These problems were addressed using a combination of mathematical morphology techniques, fuzzy systems, and *a priori* knowledge of the problems. Encouraging results were found when the results were compared with images manually segmented by expert medical doctors.

*Keywords:* ultrasound; texture; image segmentation

## 1 INTRODUCTION

The objective of this work is to develop a system for automatic segmentation of calcifications and luminal contour in intravascular ultrasound (IVUS) images as a tool to support coronary artery disease diagnosis.

Luminal contour segmentation is important because the lumen area can give the medical doctor information about the degree of vessel stenosis. On the other hand, the presence or absence of calcium demonstrated by IVUS has been shown to be an important determinant of the transcatheter intervention success.

However, in general, autonomous segmentation is one of the most difficult tasks in digital image processing. Segmentation accuracy determines the eventual success or failure of computerized analysis procedures.

In this paper, as in Brusseau's<sup>2</sup> and Bovenkamp's<sup>2</sup> works, we proposed a system for automatic luminal contour segmentation. Unlike the

Brusseau's system, our system is applied on images obtained from a rotating IVUS system due to the fact that these systems are largely used in clinical settings. Instead of a multi-agent system, as proposed by Bovenkamp, we used a simpler and powerful set of features proposed by Tuceryan<sup>3</sup> to achieve our goal of luminal contour segmentation.

Our strategy to achieve this goal is to extract local moment based texture features and a proposed pixel position feature from IVUS images to perform clustering on the basis of these features.

## 2 MATERIALS AND METHODS

In this work, we used a commercial available IVUS system (Clear View Ultra, Boston Scientific, USA). The central frequency of the rotating IVUS probe (Atlantis SR Pro, Boston Scientific, USA) was 40 MHz..

### 2.1 Moments

Our algorithm uses the moments of an image to compute texture features. The  $(p+q)$ -th order moment  $m_{pq}$  of a function of two variables  $f(x,y)$  with respect to the origin  $(0,0)$  is defined as<sup>3</sup>:

$$m_{pq} = \int_{-\infty}^{\infty} \int_{-\infty}^{\infty} f(x,y) x^p y^q dx dy \quad (1)$$

where  $p, q = 0, 1, 2, \dots$

In this paper, as in Tuceryan's work<sup>3</sup>, we regard the intensity image as a function of two variables,  $f(x,y)$ . We compute a fixed number of the lower order moments for each pixel in the input image (we use  $p+q \leq 2$ ). The moments are computed within a small local window around each pixel. Given a window size  $W$ , the coordinates are normalized to the range of  $[-0.5, 0.5]$  and the pixel is located at the center. The moments are computed with respect to this normalized coordinate system. This permits us to compare the set of moments computed for each pixel.

Let  $(i,j)$  be the pixel coordinates for which the moments are computed. For a pixel with coordinates

$(k,l)$  which falls within the window, the normalized coordinates  $(x_k, y_l)$  are given by:

$$x_k = \frac{k-i}{W} \quad y_l = \frac{l-j}{W} \quad (2)$$

Then the moment  $m_{pq}(i,j)$  within a window centered at pixel  $(i,j)$  is computed by a discrete sum approximation of Equation (1) that uses the normalized coordinates:

$$m_{pq} = \sum_{k=-W/2}^{W/2} \sum_{l=-W/2}^{W/2} f(i+k, j+l) x_k^p y_l^q \quad (3)$$

This discrete computation of the set of moments for a given pixel over a finite rectangular window corresponds to a neighborhood operation, and, therefore, it can be interpreted as a convolution of the image with a mask<sup>3)</sup>.

The set of values for each moment over the entire image can be regarded as a feature image. Let  $M_k$  be the  $k$ -th such image. If we use  $n$  moments, then there will be  $n$  such moment images. In our experiments, we used up to second order moments. That is, we used  $m_{00}, m_{01}, m_{10}, m_{11}, m_{02}, m_{20}$  which result in the images,  $M_1, M_2, M_3, M_4, M_5,$  and  $M_6$  respectively.

To enhance the discrimination power of these moments, we adopted the transformation used by Tuceryan<sup>3)</sup>. Then, we introduced a nonlinear transformation that maps moments to texture features.

Thus, we obtain the texture feature image  $F_k$  corresponding to the moment image  $M_k$  with mean  $\overline{M}_k$  using the following transformation:

$$F_k(i, j) = \frac{1}{L^2} \sum_{(a,b) \in \omega_{ij}} \left| \tanh\left(\sigma\left(M_k(a,b) - \overline{M}_k\right)\right) \right| \quad (4)$$

where:  $\omega_{ij}$  is an  $L \times L$  averaging window centered at location  $(i,j)$  and  $\sigma$  controls the shape of the function. The parameters (in Eq.4):  $\sigma$ , moment window size  $W$ , and average window size  $L$  were chosen by gradually adjusting these values and observing the resultant effect in the segmented images. The final chosen values were  $W=7, L=9$  and  $\sigma=0.01$ . They were determined empirically.

## 2.2 Luminal Contour Definition

Due to the encouraging results obtained by Tuceryan<sup>3)</sup>, the theory of moment based texture segmentation was applied to the problem of luminal contour detection in IVUS images. The system

proposed in this paper is comprised by the following modules.

**Input image.** The input image is the original image obtained from the IVUS system described in the beginning of this section.

**Feature extraction.** The feature extraction module is in charge of extraction of the transformed versions of the moments,  $F_k, k=1, 2, \dots, 6$ , and the radial distance  $R$  presented graphically in Fig.1.

In this work, we define the radial distance  $R$  as the distance from the central pixel of the image and the position of the pixel  $P$  under consideration. This distance  $R$  is normalized and becomes the seventh feature used in the following clustering of the input image pixels. The radial distance  $R$  is of fundamental importance because it helps pixels that are at similar distance from the center of the image to be included in the same cluster if they have similar texture features. The effect of using these texture and position features is that the clusters become organized in regions similar to concentric rings around the central pixel. This is associated with physiological structure of the blood vessels as represented in Fig.1. Thus, these seven features are used to comprise a feature vector for each pixel of the image.

**Clustering.** Based on their feature vectors, the input image pixels were clustered in this module using the Fuzzy C Means algorithm<sup>4)</sup>. The chosen number of clusters was four: one cluster for the region outside the vessel, one for the region between the adventitia and intima, one for the lumen and another one for the catheter zone.

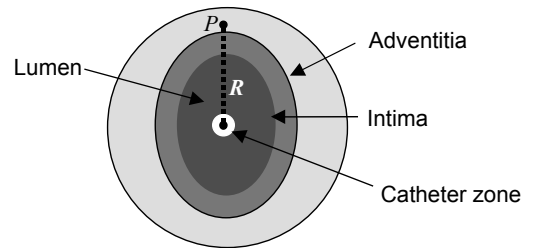


Fig.1 – Illustration of a cross section of a blood vessel

**Morphological contour smoothing.** In order to reduce the irregularities of the borders as well as some small regions around the borders, a morphological filtering is done prior to boundary detection. This filtering is performed through the application of opening and closing morphological operations with a disk structuring element of size 3.

**Boundary detection.** After the clustering and contour smoothing, the images had very well defined regions that could have their contour easily detected by traditional edge detection methods. In this system

we used the Sobel operator due to its simplicity and efficiency.

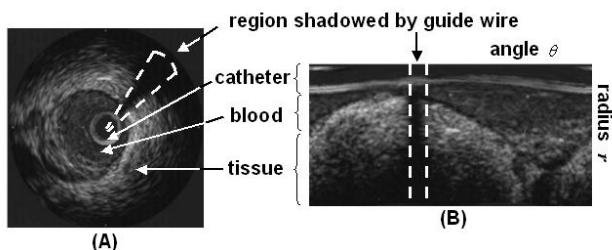


Fig.2 – Example of Cartesian coordinate system image (A) and its corresponding polar coordinate system version (B)

**Output image.** An example of the final output image can be observed in Fig.4(A).

### 2.3 The Guide Wire Shadow Problem

Sometimes due to the presence of the guide wire a region of the input image becomes shadowed and then contains no texture information. This may cause segmentation error. To solve this problem we proposed a contour correction procedure comprised of the following steps:

1) Convert the image with segmentation error from Cartesian coordinate system to polar coordinate system. An example of this process is shown in Fig.2.

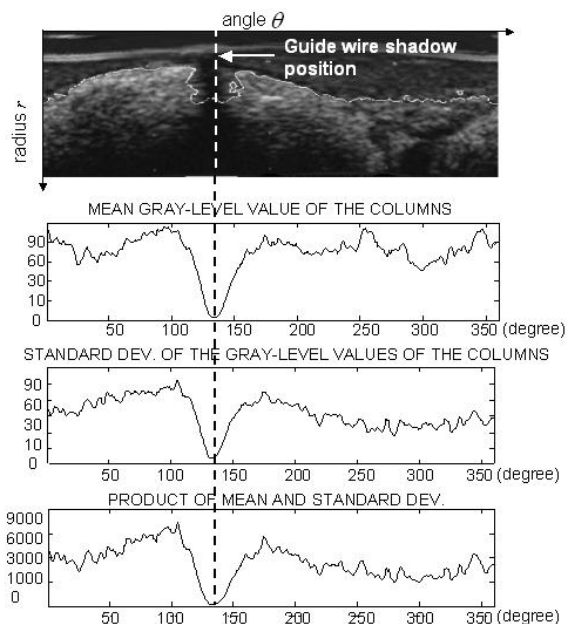


Fig.3 – Example of the search for the guide wire shadow position in polar coordinate system image based on the values of mean gray level and standard deviation of each column.

2) Automatically find the guide wire shadow. This step is carried out through the calculus of the mean gray-level and standard deviation of every column of the polar coordinate system converted image. The column which contains minimum value of the product of the mean gray-level by standard deviation is assumed to be the position of the guide wire shadowed region as illustrated in Fig.3. The catheter region was ignored during this process to avoid the influence of the ring-down artifact.

3) Erase the contour wrongly drawn in the guide wire shadow region and draw a new contour in the erased region through linear interpolation.

4) Convert the corrected image back to the Cartesian system.

## 3. RESULTS AND DISCUSSION I

Using the system presented above, tests were done with 15 *in vivo* coronary IVUS images from different patients. High correlation coefficients between the luminal contour automatically and the contour manually detected were found. These correlation coefficients values revealed preservation of standard deviation (0.92), mean gray level (0.89), and area (0.87) in the regions automatically segmented. An example of the results is shown in Fig.4 together with the image segmented by a medical doctor for comparison.

Our preliminary tests suggest that the moment based texture features together with the radial distance are feasible components for a feature vector in IVUS image segmentation when the aim is to find the luminal contour. A contour correction procedure based on the mean gray level and variance of each column of the polar coordinate version of the input image was presented as a feasible solution for the problem of error generated by the guide wire shadow.

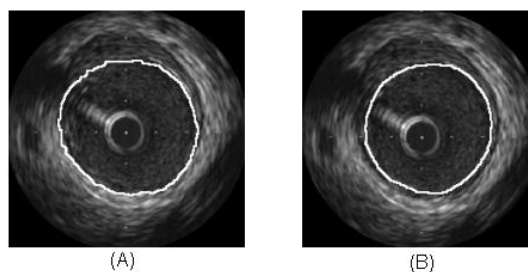


Fig.4 – Example of luminal contour detection. (A) and (B) are the same images obtained from patient A. (A) Automatically defined contour. (B) manually defined contour

## 4. CALCIFICATION DETECTION

One of the characteristics of the calcification regions is that they usually present high intensity echo for IVUS images. This fact makes it possible to segment calcified regions by gray level threshold techniques. However as the intensity level change from image to image it is quite difficult to find a single threshold level that could provide an accurate segmentation for a large group of images. Thus, it is necessary to adapt the threshold level to every single image.

### 4.1 Adaptive Threshold Estimator

Otsu<sup>5)</sup> developed an optimal threshold selection method based on the maximization of the separability of the resultant classes. Thus, due to its simplicity and efficiency Otsu's method was used as threshold estimator in this segmentation algorithm.

The process of threshold selection presented is iteratively used to automatically generate threshold values for multiscale segmentation. For such automatic process, the following algorithm was implemented:

Step 1: Compute the histogram.

Step 2: Compute the optimal threshold.

Step 3: Compute a new histogram for the image with gray levels greater than the threshold.

Step 4: Go to step 2

After perform several tests, it was observed that two iterations of the above algorithm were sufficient to obtain an approximate segmentation of the regions of calcification that will be considered region of interest (ROI).

### 4.2 Identification of Calcification from the ROIs

Together with the intensity, another characteristic of the calcification regions is that they are usually followed by an acoustic shadow due to the strong reflection of the ultrasound beam in these regions.

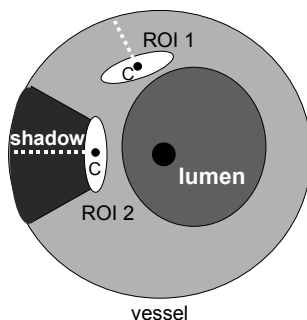


Fig.5 – Example of identification of calcification acoustic shadow .

Thus an efficient way to decide whether a given ROI is a calcification region or not is through analysis of the region posterior to this ROI. As shown in Fig.5.

We can observe in Fig.5 that the region of calcification (ROI 2) is followed by an acoustic shadow and then will present a level for median of the gray level values (in the dotted line) lower than the one of ROI 1.

Thus, in order to detect the acoustic shadow and then determine whether a given ROI is calcification or not, the following algorithm was constructed:

Step 1: Determine the centroid  $C$  of the ROI.

Step 2: From the centroid of the ROI to the outer boundary of the image, calculate the median gray level value  $Med$ .

Step 3: If  $Med \leq T_{med}$  than classify the ROI as calcification. Else, classify ROI as non-calcification

$T_{med}$  was chosen based on tests with several images.

## 5. RESULT AND DISCUSSIONS II

Using the algorithms for adaptive thresholding and acoustic shadow detection tests were done. Varying the threshold  $T_{med}$  in the range from 10 to 200 and observing the number of true positive and false positive, a receiver operating characteristic (ROC) curve was constructed. It is shown in Fig.6. The area under the curve (AUC) is equal to 0.87. For the chosen  $T_{med}=25$  the rate of true positive was 84% and the rate false positive was 12%. Thus, we had sensitivity = 0.84 and specificity = 0.88.

## 6. CONCLUSIONS

Otsu's algorithm for threshold selection has been successfully applied for segmentation of calcification regions in IVUS images. However, some bright regions of normal tissue are also, often, segmented. Then an algorithm for identification of the ROIs that are really regions of calcification was implemented taking as identification criteria the presence or absence of acoustic shadow. A ROC curve was plotted showing the performance of the proposed algorithm.

A moment based texture feature together with a position feature presented encouraging results in luminal contour detection . As future works we plan

to expand the algorithms for detection of vessel contour and other kind of plaques.

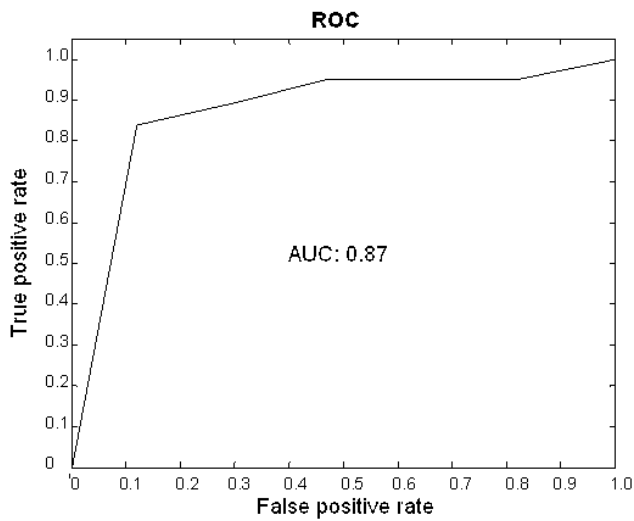


Fig.6 – Receiver Operating Characteristic (ROC) curve.

## REFERENCES

- 1) E. Brusseau *et al*, Fully automatic luminal contour segmentation in intracoronary ultrasound imaging – a statistical approach, *IEEE Trans. on Medical Imaging*, Vol. 23, No. 5, pp.554-566, (2004)
- 2) E.G.P. Bovenkamp *at al*, Multi-agent segmentation of IVUS images, *Pattern Recognition*, Elsevier, Vol. 37, pp. 647-663, No. 4, (2004)
- 3) M. Tuceryan, Moment based texture segmentation, *Proceedings of 11th IAPR International Conference on Image, Speech, Signal Analysis and Pattern Recognition*, pp.45-48, (1992)
- 4) J.C. Bezdek, *Pattern recognition with fuzzy objective function algorithms*, Plenum Press, New York, (1981)
- 5) N. Otsu, A threshold selection method from gray-level histograms, *IEEE Trans. on Systems, Man, and Cybernetics*, smc-9, pp.62-66, (1979)